PAPER • OPEN ACCESS

The root cause of disruptive NTMs and paths to stable operation in DIII-D ITER baseline scenario plasmas

To cite this article: L. Bardoczi *et al* 2024 *Nucl. Fusion* **64** 126005

OPEN ACCESS
IOP Publishing | International Atomic Energy Agency
Nuclear Fusion
Nucl. Fusion **64** (2024) 126005 (11pp)
https://doi.org/10.1088/1741-4326/ad7787

The root cause of disruptive NTMs and paths to stable operation in DIII-D ITER baseline scenario plasmas

L. Bardoczi[1,2,*], N.J. Richner[3], N.C. Logan[4,5], E.J. Strait[1], C.T. Holcomb[4], J. Zhu[6] and C. Rea[6]

[1] General Atomics, San Diego, CA, United States of America
[2] University of California, Irvine, CA 92697, United States of America
[3] Oak Ridge Associated Universities, Oak Ridge, TN, United States of America
[4] Lawrence Livermore National Laboratory, Livermore, CA, United States of America
[5] Columbia University, New York, NY, United States of America
[6] Plasma Science and Fusion Center, MIT, Cambridge, MA, United States of America

E-mail: bardoczil@fusion.gat.com

Received 1 July 2024
Accepted for publication 4 September 2024
Published 23 September 2024

Abstract

Analyses of the DIII-D ITER Baseline Scenario database support that the disruptive m,n=2,1 magnetic islands are pressure gradient driven, non-linear instabilities seeded in a sequence of stochastic transient magnetic perturbations, and that the current profile relaxation does not affect the m,n=2,1 island onset rate. At low torque, these Neoclassical Tearing Modes are most commonly seeded by non-linear 3-wave coupling when the differential rotation between the q=1 & q=2 rational surfaces approaches zero. Lack of statistically significant difference between the current profiles of stable and unstable states, as well as lack of correlation between the tearing mode onset rate and the current profile relaxation both reject causality between the current profile evolution and the 2,1 magnetic island onsets in these plasmas. These support that preserving the differential rotation between the q=1 and q=2 rational surfaces is key to long pulse stable operation in the plasma scenario planned for ITER, while optimization of the current profile within the explored parameter space may lead to much weaker improvements than sustaining the differential rotation.

Keywords: tearing, stability, tokamak, MHD

(Some figures may appear in colour only in the online journal)

1. Introduction

Neoclassical tearing modes (NTMs) characterized by $m = 2$ poloidal and $n = 1$ toroidal mode numbers are the primary limiting instabilities of low-torque DIII-D H-mode scenarios run with the ITER normalized parameter set and shape (IBS or ITER baseline scenario). Although much work has been done to stabilize the scenario in DIII-D by adjusting the auxiliary heating [1] and using Electron Cyclotron Current Drive (ECCD) [2], understanding the root cause of these resistive modes is essential in order to develop and project stable operating solutions to ITER and beyond. The Modified Rutherford Equation (MRE, [3]) predicts the onset of a robustly growing NTM as a result of a temporal imbalance between stabilizing and destabilizing mechanisms. At fixed plasma pressure such an imbalance could occur for example due to the current profile becoming more unstable (or less stable), or due to

* Author to whom any correspondence should be addressed.

weakening of the stabilizing polarization current, for example due to rotation profile flattening. Rotation has been widely recognized to be critical for enhancing tearing stability in tokamak experiments [4–6]. This paper presents statistical analyses investigating possible physical mechanisms of disruptive $m,n = 2,1$ instability onsets, namely the role of the equilibrium rotation and current profiles.

In the DIII-D IBS database, the 2,1 tearing modes are most commonly triggered at the time and frequency of a sawtooth precursor, often coupled to core $n > 1$ islands, when the differential rotation approaches zero. This strongly supports that the sawtooth precursor and the rotation profile flattening is the 'cause in fact' of the 2,1 island onsets. On the other hand, lack of statistically significant differences between the current profile of stable and unstable states and lack of correlation between the tearing mode onset time distribution and the current profile relaxation both support that a causal relationship between the current profile evolution and the 2,1 magnetic island onsets is highly unlikely. These imply that magnetohydrodynamic transients and polarization current physics lie at the roots of disruptive 2,1 NTMs in the DIII-D ITER baseline scenario.

2. 2,1 NTM seeding by non-linear 3-wave coupling

In the DIII-D IBS discharges at low torque ($T < 1$ Nm), most $m,n = 2,1$ NTM seed islands are formed either by the sawtooth precursor and/or by frequency matching helical magnetic modes that satisfy the mode number resonance condition, for example by the coupling of $m,n = 1,1$ sawtooth precursor to a preceding $m,n = 3,2$ island [7, 8]. The representative discharge in figure 1 is characterized by ELM events and sawtooth crash events, both of which are known to be able to trigger NTMs [9, 10]. In the analysed timeframe, the normalized plasma beta (β_N) is held constant and the current profile has fully relaxed. At the time of the $m,n = 2,1$ island seeding (marked by a vertical dashed line in figure 1) there is no ELM and the expanded view in figure 1(c) shows that there is no sawtooth crash either. Three modes participate in the 2,1 seeding: a 1,1 sawtooth precursor, a 4,3, island and a 3,2 island. The perturbed poloidal magnetic field (B_p) spectrogram in figure 1(a) shows that the 1,1 mode near $f_{1,1} = 3.7$ kHz frequency grows and crashes periodically. The sawtooth frequency at the 2,1 formation is marked by the lower horizontal dashed line. In addition, the second and third harmonic frequencies are also marked with dashed horizontal lines in figure 1(a). The 3,2 island rotates with a stable frequency near the second harmonic frequency of the sawtooth and the 4,3 island slows from a maximum frequency of about $f_{4,3} = 14$ kHz to about the third harmonic frequency of the sawtooth by the time of the 2,1 NTM seeding event.

Clearly, the 2,1 island forms when the 4,3 couples to the 3,2 and the 1,1. This is consistent with the 1,1 being driven by the coupling between the 4,3 and the 3,2, while the 1,1

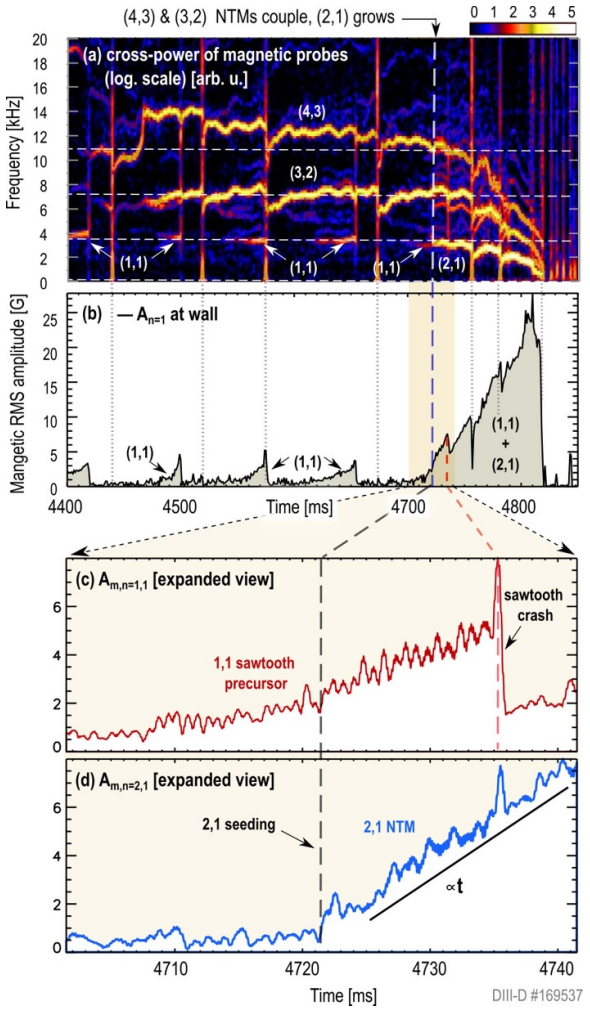

Figure 1. (a) Cross-power spectrogram of magnetic fluctuations. (b) $n = 1$ magnetic amplitude. Expanded view of (c) $m,n = 1,1$ and (d) $m,n = 2,1$ amplitudes. Reprinted figure with permission from [7], Copyright (2021) by the American Physical Society.

and coupled 3,2 produce the 2,1 seed island. These three-wave interactions satisfy the following relations at $f_{m,n}/n =$ constant:

$$(m,n=4,3) - (m,n=3,2) \rightarrow (m,n=1,1), \quad (1)$$

$$(m,n=3,2) - (m,n=1,1) \rightarrow (m,n=2,1). \quad (2)$$

To determine if the 2,1 island is seeded by the sawtooth crash, or by the coupling during the sawtooth precursor, we identify the 2,1 onset time more accurately by isolating the odd ($m = 1$) and even ($m = 2$) poloidal components of the $n = 1$ modes by simultaneous measurements of B_p in the high-field-side and in the low-field-side midplane via Mirnov-probes [11]. The resulting B_p amplitude of the 1,1 mode in figure 1(c) and the 2,1 amplitude in figure 1(d) show that at the time of the 2,1 onset the 1,1 mode does not crash, clarifying that the 2,1 island is not seeded by a sawtooth-crash. The 2,1 island grows linearly in time, which is consistent with the bootstrap current dominated asymptotic solution of the MRE

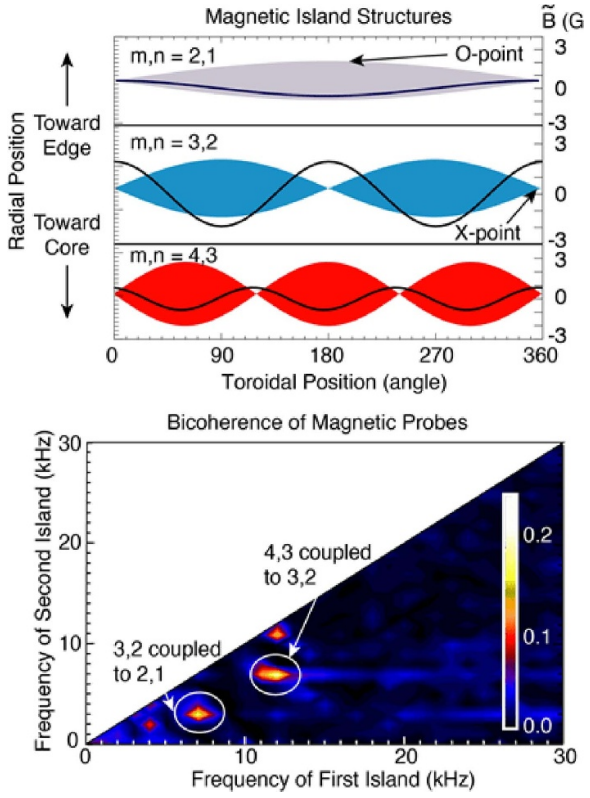

Figure 2. (*b*) Bi-coherence of B_θ at the time of 2,1 seeding. (*c*) Spatial harmonics of B_θ and cartoon of the associated 2,1, 3,2 and 4,3 islands with phasing derived from B_θ. Reprinted figure with permission from [7], Copyright (2021) by the American Physical Society.

[12], i.e. the 2,1 island is neoclassiacally driven. In addition, bi-spectral analysis using all available Mirnov-probes located in the outboard mid-plane confirms that the participating modes are phase-locked at the time of seeding [7, 8], see figure 2, as predicted by analytic theory [13]. The magnetic energy balance shows that the amplitude of the 4,3 mode decreases when the 2,1 seeding occurs, while the amplitude of the 3,2 mode remains relatively constant [7, 8]. This observation is consistent with the magnetic energy of the 4,3 mode converting into the formation of the 2,1 seed, according to equations (1) and (2).

Extending this analysis to a database of 144 DIII-D ITER baseline scenario discharges shows that the frequency matching condition between resonant islands is satisfied in more than 70% of the plasmas at the time of 2,1 NTM onsets. This supports that the three-wave coupling is the most common seeding mechanism of disruptive 2,1 NTMs in these plasmas. The fact that the three-wave relations can drive islands with and without phase-locking, but robustly growing 2,1 NTMs are triggered only when the modes are rotationally coupled, i.e. when the rotation profile is flat, suggest that the rotation profile has a key role in enabling the three-wave driven island to surpass the NTM threshold. In terms of the modified Rutherford equation, the importance of differential rotation is expected due to stabilizing polarization currents, which arise when the driven seed island frequency significantly differs from the local plasma rotation. This occurs, when the driving modes rotate at different frequencies, i.e. when the rotation profile is steep. Furthermore, rotation shear is recognized for its screening effect on non-axisymmetric magnetic perturbations. Therefore, the flattened rotation profile also facilitates the seeding event by promoting the penetration of magnetic perturbations of the triggering modes to the 2,1 surface. We will examine the role of the rotation profile in sections 4 and 5.

3. The 2,1 NTM onset statistics and it is consequences

2,1 tearing modes can be driven both by the current and the pressure gradient, as per the modified Rutherford equation (MRE). Given that the pressure is kept fixed in H-mode but the current evolves over several current relaxation times ($\tau_R \sim 0.6$ s) into the IBS H-mode pressure flattop, the onset of classically driven tearing modes must be correlated to the current profile relaxation. We analyse the tearing mode onset time distribution in order to determine if the 2,1 tearing modes are affected by (i) parameters that evolve nearly the same way in repeat shots (such as the current profile evolution due to resistive diffusion driven relaxation), (ii) or by a combination of parameters that are held fixed (such as the plasma beta) and randomly varying parameters (such as the rotation in the presence of core islands). This analysis includes both rotating and born locked modes. We report in figure 3(*a*) that the 2,1 onset times ($-d\mathrm{N}/d\mathrm{t}$) follow an exponential distribution within the β_N flattop in a database of 144 IBS discharges (including both low and high torque). Here we use $\Delta\tau = 500$ ms for binning the distribution function, which is much larger than the ELM and sawtooth periods. In addition, the distribution of surviving shots ($N(t)$, the number of shots that have survived until time t) is reported in figure 3(*b*). The ratio $\lambda = (-\mathrm{d}N/\mathrm{d}t)/N$ is the onset rate, reported in figure 3(*c*). λ is the fraction of 2,1 onsets in a given time window relative to the number of shots surviving up to that time.

It is interesting to note that most modes occur soon after the plasmas reach the pressure flattop, during the first current relaxation period ($\tau_R \sim 600$ ms), which makes it appear as if the plasmas were the most unstable during this time. However, the onset time distribution is not the correct metric of the stability, but instead the number of shots going unstable relative to the remaining sample size, i.e. λ, is the correct metric of stability. We elucidate this by briefly reflecting to the example of the radioactive decay, whose stability properties are constant in time. Consider that the activity ($-\mathrm{d}N_R/\mathrm{d}t$) decays exponentially over time, but the sample stability is given by the constant decay rate (λ_R). Due to the relationship between the onset time distribution and the onset rate, constant λ implies expo-

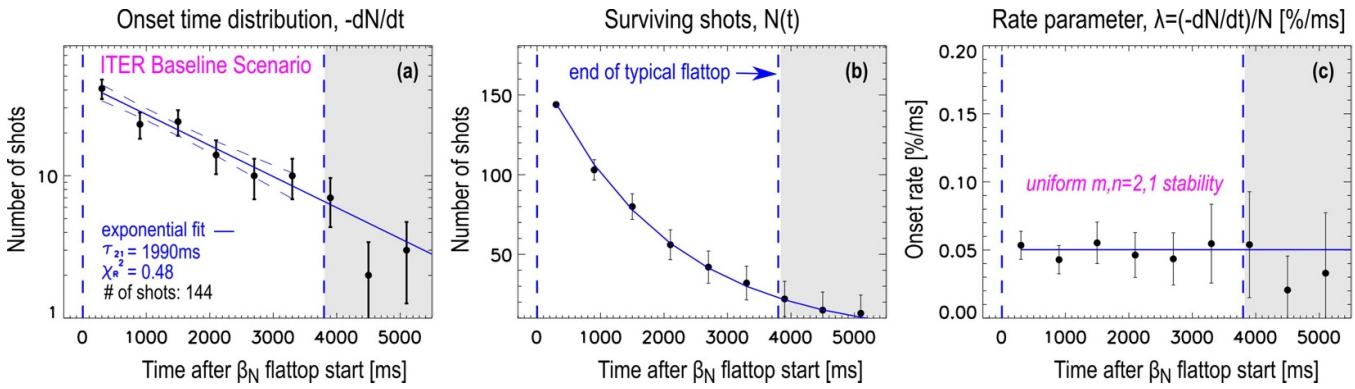

Figure 3. (*a*) Onset time distribution, (*b*) surviving shot distribution and (*c*) onset rate of 2,1 NTMs in the DIII-D IBS.

nential onset time distribution and vice versa. If the stability was worsening (improving) in time, then λ would be increasing (decreasing) as a function of time. Consequently, the onset time distribution would decay faster (slower) than exponential. Since λ is constant, it is clear that the plasma stability is constant in time and therefore it is not correlated with the current profile relaxation. The fact that the onset is uncorrelated to the current profile evolution supports that classical tearing mode physics does not play an important role in the onset of these instabilities.

The fact that both dN/dt and $N(t)$ are exponential strongly supports that the 2,1 tearing mode onset is governed by a Poisson point process, which implies that the modes exhibit a finite threshold and are triggered at random times with near uniform probability in time. This is in qualitative agreement with the modified Rutherford equation (MRE) of NTMs, where the instability is triggered when a seed island's width (produced by a transient MHD) exceeds the NTM threshold. This threshold is provided by net stabilization at zero island width via classical physics, polarization currents, finite cross-field transport and other small island terms. In regard to the MRE, the onset occurs due to an imbalance between the stabilizing and destabilizing terms, leading to a seed island larger than the NTM threshold. Such an imbalance can occur if, for example the stabilization from polarization currents suddenly decreases due to rotation profile flattening. The fact that the onset conditions (sawtooth precursor with low differential rotation often coupled to $n > 1$ islands) occur at random times within the flattop indicates that NTM driving and stabilizing terms must be part of a chaotic system. Such a chaotic system can arise for example by $n > 1$ tearing modes that non-linearly interact with the fast ion population and thereby cause rotation profile flattening and concomitant weakening of stabilizing polarization currents at random times. Such non-linear interactions between core $n > 1$ islands and the fast ions have been reported in integrated TRANSP-Kick simulations of DIII-D IBS plasmas [14].

We note that the reported exponential onset time distribution of 2,1 NTMs in the DIII-D IBS is consistent with previous work [1], although the interpretation given here differs from the interpretation given in [1]. Further, the reported onset statistics matches observations of various types of H-modes in a database of over 1,400 unstable H-mode discharges in DIII-D [15], suggesting that the physics lessons learned in the ITER baseline scenario will be pertinent to many other plasma scenarios as well.

4. 2,1 NTM onset frequency dependence on plasma pressure, differential rotation, current profile and effective charge

In this section, we investigate the effect of (i) β_N, motivated by modified Rutherford equation which predicts that NTMs grow due to the pressure gradient driven bootstrap current, (ii) the differential rotation ($\Delta f_{1,2}$), motivated by the observation of three-wave seeding at flat rotation profiles and (iii) $\nabla j_{\parallel}$ to measure the possible role of the classical drive and (iv) the effective charge ($Z_{\rm eff}$) to characterize the effect of impurities in the onset of the 2,1 islands. Here, the parallel current gradient at is provided by CAKE (Consistent Automatic Kinetic Equilibrium reconstruction). As the IBS is defined by a relatively narrow β_N range, recovering the pressure dependence within the scenario is not possible. Thus, we expand the database of this analysis to all types of H-mode discharges that are characterized by low edge safety factor in the $2 < q_{95} < 3.7$ range. We calculate the onset empirical probability $P(X^i)$ in a database of 7014 stable and 697 unstable H-mode discharges following the procedure given in [16]. First, we create a stable and an unstable database of time-slices by dividing the H-mode of every plasma into $\Delta\tau = 100$ ms time windows (points). The point right before a 2,1 islands onset are classified 'unstable'. Point preceding the unstable points as well as all points of stable discharges are classified as 'stable'. Next, the empirical probability is calculated using these two subsets as $P(X^i) = H_u(X^i)/H_t(X^i)$. Here $H_u(X^i)$ and $H_s(X^i)$ are the histograms of X^i parameters calculated from the unstable and stable databases, respectively (hence the 'u' and 's' indices), and $H_t(X^i) = H_u(X^i) + H_s(X^i)$ is the histogram of the union of the stable and unstable databases. All histograms are calculated in 35 points with respect to X^i. The ranges of the X^i parameters are chosen to cover more than 95% of the H-mode operational space. The uncertainty of each point in H_u and H_s are calculated as $\sqrt{N}$, where N is the number of time-slices in a given bin. Gaussian error-propagation is then used to calculate the uncertainty of the total distribution and the uncertainty

of $P(X^i)$. Missing data is considered as 'missing completely at random'.

Figure 4 shows $H_t(X^i)$ (grey) and $P(X^i)$ (red) with respect to β_N, $\Delta f_{1,2}$, and $\nabla j_{\|}$. $P(\beta_N)$ in figure 4(*a*) strongly increases with β_N in the $\beta_N > 2.0$ operational space, which is a characteristic dependency of pressure gradient driven magnetic islands, i.e. NTMs, in the $\beta_N < 3.5$ range. P shows significant variation as well with respect to $\Delta f_{1,2}$ (figure 4(*b*)). The plasma is most sensitive to the differential rotation in a narrow range near $\Delta f_{1,2} = 0$ kHz, showing that flat rotation profiles are prone to 2,1 onset at low q_{95}. Interestingly, the change of P within the entire range of $\nabla j_{\|}$ and Z_{eff} is comparable to the uncertainty of the points. If classical stability is affected significantly by the current relaxation, then a correlation between the mode onset and $\nabla j_{\|}$ should be seen in the data. Thus, the effect of the current profile on the 2,1 tearing stability appears to be weak in this database. This is in line with the conclusion of section 3 reporting that the 2,1 onset rate is unaffected by the current profile relaxation. These results are in good agreement as well as with [17] where low rotation shear was reported to have a strong effect on the tearing onset, while the current profile does not. In agreement, previous work on various tokamaks, such as the ASDEX-Upgrade [4], TCV [5] and NSTX [6], reported the sensitivity of tearing stability to the rotation profile. Finally, the flat $P(Z_{\text{eff}})$ graph in figure 4(*d*) indicates that impurities do not have a significant effect on the 2,1 NTM onset in DIII-D.

5. 2,1 NTM onset isolation in the parameter space of differential rotation and rotation shear

The effect of the differential rotation ($\Delta f_{1,2}$) and the rotation shear are investigated in the IBS database by the stability diagram in figure 5(*a*), which uses ZipFit profiles fitted to charge exchange recombination data (CER, [18]). Here three types of points are used to populate the map. As in section 4, first the pressure flattop of each stable and unstable plasma is divided into short time-slices ($\Delta\tau = 20$ ms in this analysis to avoid averaging over rapidly changing rotation profiles). All time-slices of the stable plasmas are shown with blue points. The stable time-slices of unstable plasmas (i.e. times within the unstable plasmas preceding the instability onset) are shown with magenta points. Finally, the last time slices right before the instability growth ('onset times') are shown with yellow points.

The instability onset points cluster away from the centre of the stable points' cluster (both of those of the stable and unstable plasmas). Accordingly, the one-dimensional normalized histograms in figures 5(*b*) and (*c*) show that the mean of the distribution of the onset times (yellow) is well separated from the mean of the distribution of the stable time-slices (blue and magenta). Most unstable points are located near $\Delta f_{1,2} \sim 0$ kHz (± 1 kHz), while the distributions of stable time points peak near $\Delta f_{1,2} \sim 1.5$ and $\Delta f_{1,2} \sim 2.0$ kHz and have standard deviations $\sigma \sim 0.5$ kHz. Some overlap exists between the onset and stable distributions; however, the isolation of the mean values is greater than 2σ, in qualitative agreement with figure 4(*b*) of section 4. In terms of the rotation shear, it appears that most modes occur when the rotation profile has become hollow, i.e. the shear at the $q = 3/2$ surface is positive. We note that in a few cases, the 2,1 NTM onset occurred at high differential rotation and negative rotation shear. These cases must have different origins than rotation flattening or hollowing, for example inadequate error field

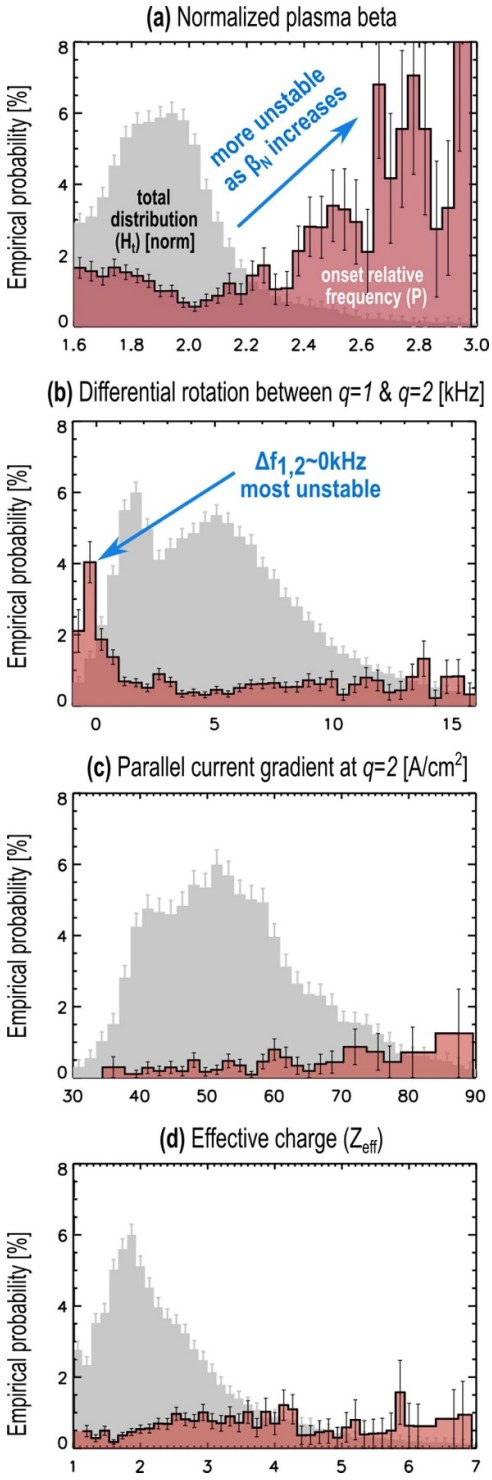

Figure 4. Total distribution (grey) and onset relative frequency of 2,1 tearing modes (red) in the β_N flattop of H-mode plasmas in the $q_{95} = 2.9$–3.2 range as a function of (*a*) β_N, (*b*) $\Delta f_{1,2}$, (*c*)$\nabla j_{\|}$ and (*d*) Z_{eff}.

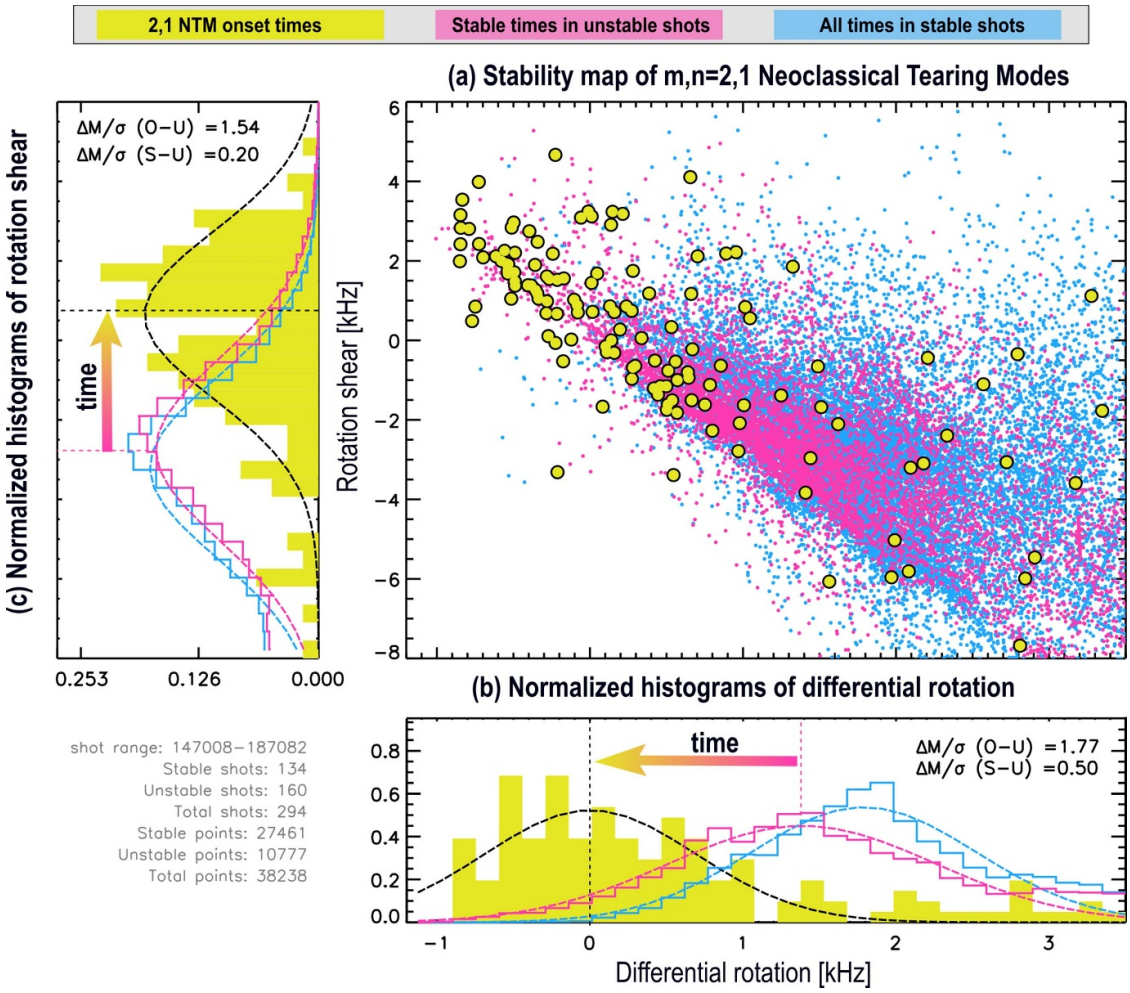

Figure 5. (*a*) Stable, unstable and 2,1 NTM onset points in the parameter space of differential rotation and rotation shear. Normalized distribution functions of (*b*) differential rotation and (*c*) rotation shear at $q = 1.5$. The separation of the distributions (ΔM) relative to the standard deviation (σ) are printed in (*b*) and (*c*) separately for the onset and unstable databases (O-U) and the stable and unstable databases (S-U).

correction, inadequate density control, a sudden change in the current profile, etc.

Differences between the stable and unstable rotation ($f(r)$) and differential rotation ($\Delta f_{1,2}(r)$) profiles are further characterized in figures 6(*a*) and (*b*), respectively. Here the solid lines represent the ensemble averaged radial profiles of automatic ZipFit fits to the CER carbon impurity rotation data within each group of points (onset times (black), stable times within unstable shots (magenta) and all times of stable shots (blue)), while the error-bars (or shading) represent the standard deviation within each group (σ). The calculation is performed separately for each group of points. For example, the ensemble averaged rotation profile and its standard deviation in the stable database:

$$\langle f(r)\rangle_s = \frac{1}{N_s}\sum_{k=0}^{N_s}(f_k(r)) \text{ and}$$
$$\sigma_s(r) = \sqrt{\frac{\sum_{k=0}^{N_s}(\langle f(r)\rangle - f_k(r))^2}{N_s}}. \quad (3)$$

Here $f_k(r)$ is the radial profile of the rotation in a stable time window and N_s is the number of stable time-slices. $<f(r)>$ in figure 6(*a*) shows that the rotation is nearly flat between the $q = 1$ and $q = 2$ surfaces right before the instability onset, while it is steep in stable plasma conditions. Figure 6(*b*) shows that the separation between the stable and unstable $\Delta f_{1,2}(r)$ is more than 2σ at $q = 1$.

Overall, it can be concluded that the rotation profile undergoes significant changes right before the 2,1 islands destabilize. These changes are evident both in the rotation shear and in the differential rotation. The strong correlation and the chronological order between the rotation profile flattening and the 2,1 island onset supports that rotation flattening can be the cause of the 2,1 instability onset.

6. The current profile does not isolate the 2,1 instability onset

Next, we analyse the radial profile of the Motional Stark Effect data (MSE, [19]), which is used by equilibrium reconstruction

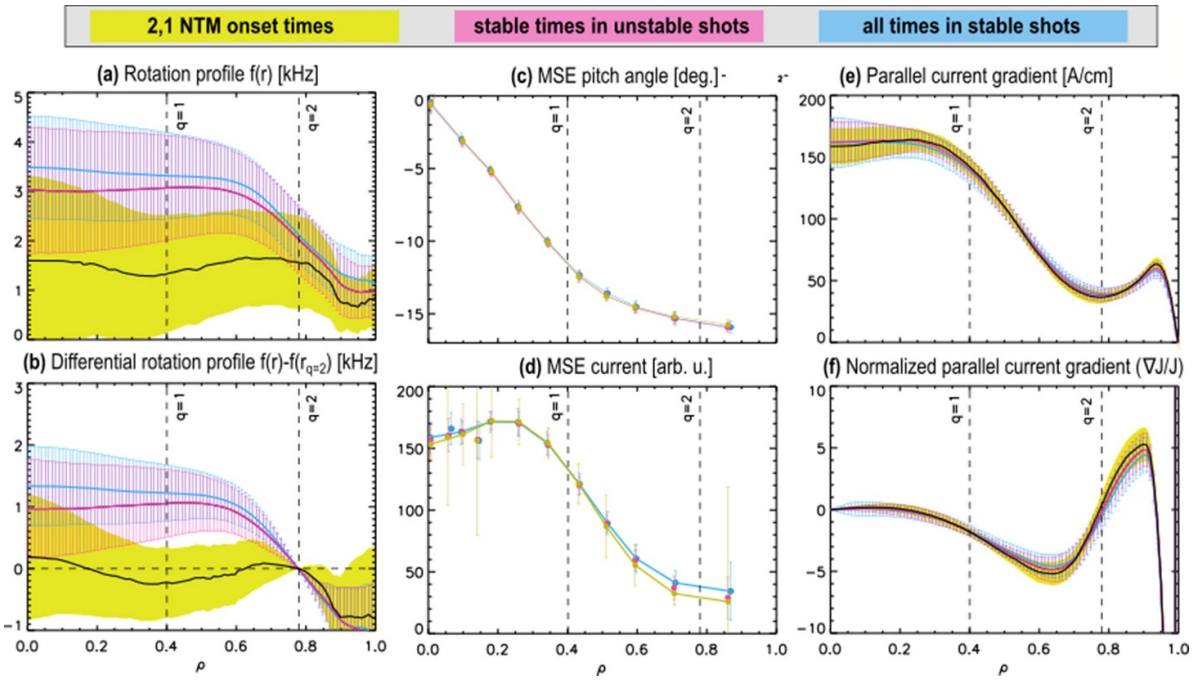

Figure 6. (*a*) Rotation profiles and (*b*) differential rotation profiles. (*c*) MSE pitch angle profiles and (*d*) MSE current profiles. (*e*) Parallel current density profiles and (*f*) normalized parallel current density gradient profiles in magnetic equilibrium reconstructions. Each figure shows the ensemble averaged profiles and their standard deviations for (i) the 2,1 NTM onset times (yellow), (ii) for stable times within plasmas that eventually became unstable (magenta) and (iii) in fully stable plasmas (blue).

codes, such as EFIT to internally constrain the shape of the plasma current profile. Using the same groups of time-slices as defined in section 5, i.e. (i) stable shots, (ii) stable part of unstable shots and (iii) onset times, the ensemble average and the standard deviation of the MSE pitch angle (γ) profile are shown in figure 6(*c*). These profiles show that there are no statistically significant changes in the measured γ profiles between stable and unstable times. Next, using γ, we approximate the current density (j) in figure 6(*d*) as in a previous work [20]. This analysis shows that differences between the MSE current density profiles in the stable and unstable time-slices are statistically insignificant.

In addition, we show the parallel current density and its normalized gradient in figures 6(*e*) and (*f*), respectively, calculated from the exact same equilibrium reconstructions as those used in a previous work [21], which utilize both external magnetic data and internal MSE data. These profiles also demonstrate that differences between the current profiles of the stable and onset unstable are statistically insignificant. These current density profiles exhibit a local minimum near $\rho = 0.8$ due to the combined effect of the edge bootstrap current and the core inductive current. This minimum is referred to as the current 'well'. Here the normalized current gradient inside of the current 'well' is defined as $\nabla j/j_{\text{in}} = (j_{\text{well}} - j_{\text{ped}})\,/(\rho_{\text{well}} - \rho_{\text{ped}})\,/j_{\text{well}})$ and the normalized current gradient outside the well is defined as $\nabla j/j_{\text{out}} = (j_{\rho=0.5} - j_{\text{well}})/(0.5 - \rho_{\text{well}})\,/j_{\rho\,=\,0.5})$. Here j_{well} is the current density at the bottom of the current well whose location is denoted by ρ_{well}, while j_{ped} is the current density at the pedestal top whose location is denoted by ρ_{ped}.

In comparison, we note that these results are consistent with figure 5 of [21], which shows that the separation between the stable and unstable distribution functions of $\nabla j/j_{\text{out}}$ equals to about half of the standard deviation (the same holds for $\nabla j/j_{\text{in}}$).

We plot the stability map in the $\nabla j/j_{\text{in}}$ and $\nabla j/j_{\text{out}}$ parameter space as well as the normalized distribution functions of $\nabla j/j_{\text{in}}$ and $\nabla j/j_{\text{out}}$ in figure 7. This map shows that the mean value of the two stable distributions is different by less than 0.5 σ, while the mean of the onset distribution differs only by about 0.5–0.6 σ. Thus, the distributions of the normalized parallel current density gradient greatly overlap, and a fully stable region does not exist in their space. This agrees with figure 5 of [21] except that here (figure 7(*a*)) all 2,1 NTM onsets of the database are shown from a larger IBS database than that discussed in [21].

A more recent work to optimize the stability reported that changing the fuelling and the heating program of the discharge can lower the pedestal current by about one standard deviation in these plasmas which lowers the modelled tearing index (Δ') and raises the modelled tearing threshold (Δ'_c) [22]. Since Δ'_c is in arbitrary units in the simulations of [22], there is no definitive evidence that a zero crossing occurs in the experimental range of $\nabla j/j_{\text{out}}$ (majority of the shots, i.e. 1-sigma events, fall in the narrow range of $\nabla j/j_{\text{out}}$ ~3–5). On the other hand, analytic theory predicts that 2,1 tearing modes are classically stable in this scenario [23]. Therefore, given the available current profile measurements, simulations and analytic theory, it is most plausible that the typical changes of the current profile are too small to cause the mode onset in this scenario, in agreement with the measured constant 2,1 NTM onset rate during

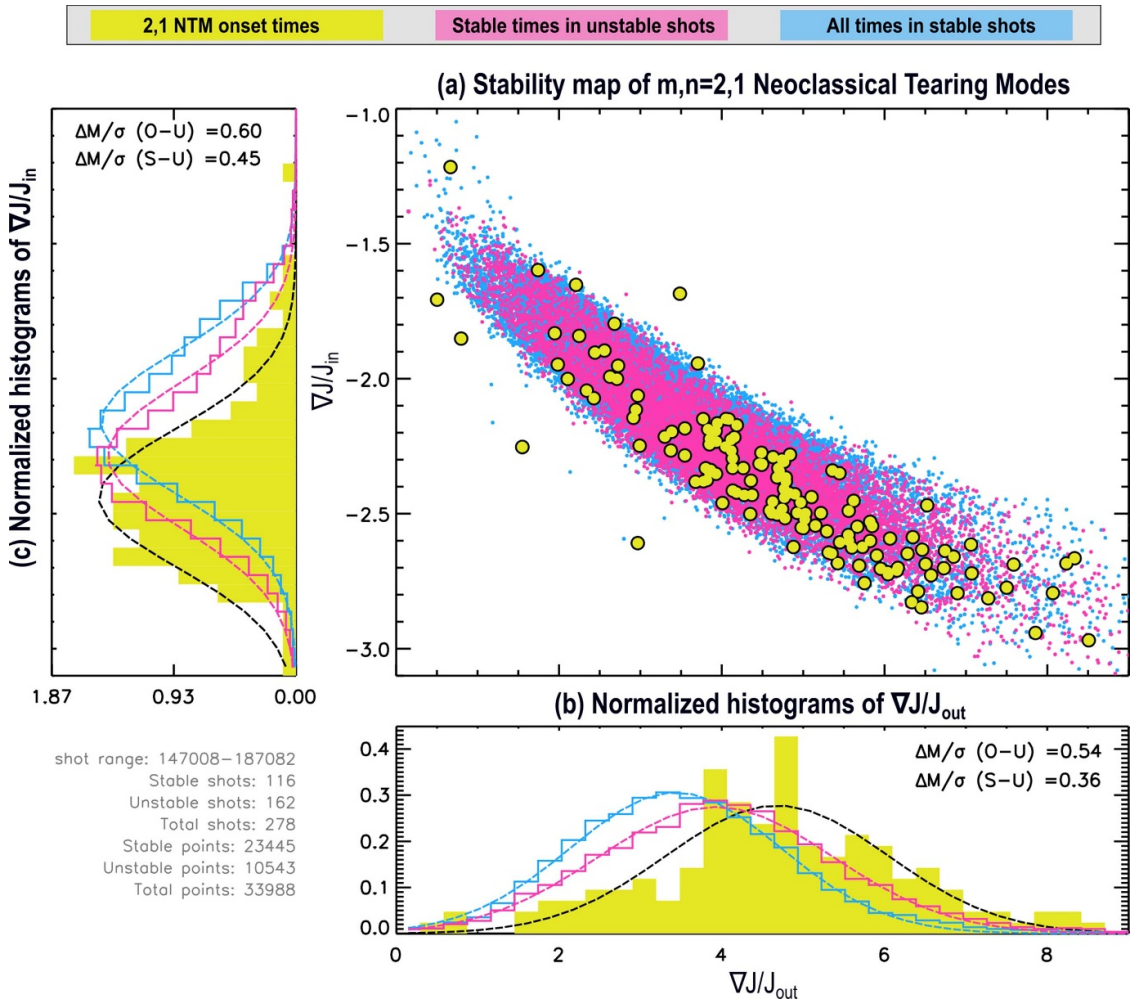

Figure 7. Stable, unstable and 2,1 NTM onset points in the parameter space of $\nabla J/J_{\rm in}$ and $\nabla J/J_{\rm out}$. Normalized distribution functions distribution functions of (b)$\nabla J/J_{\rm in}$ and (c)$\nabla J/J_{\rm out}$. The separation of the distributions (ΔM) relative to the standard deviation (σ) are printed in (b) and (c) separately for the onset and unstable databases (O-U) and the stable and unstable databases (S-U).

the current relaxation which directly shows that the stability of these modes is not affected by the associated changes of $j_{\|}(r)$ (reported in section 2).

Importantly, there are no known current measurements that can predict the mode onset time within the unstable discharges. To demonstrate this, example time traces of the parallel current, the differential rotation, and the $n = 1$ magnetic RMS amplitude are shown in figure 8. These time traces clearly demonstrate that the differential rotation approaches zero before the 2,1 NTM onset. While the mean value of the current density at $q = 2$ is different in some of these examples, their time traces do not take a special value before the modes destabilize, i.e. the current density has no predictive value for the onset of the 2,1 NTMs. In the absence of temporal correlation between the current density and the instability onset, there is no clear evidence that the current profile evolution would be the cause of the 2,1 NTM onset. Thus, within experimental uncertainties, causality between the current evolution and the 2,1 NTM onset can be rejected. This is in agreement with modelling an analytic theory as discussed above.

7. The rotation and current profiles are uncorrelated

As it has been shown that $\Delta f_{1,2}$ is correlated to the 2,1 tearing mode onsets (section 5), but the pitch angle and current density data are not (section 6), it follows that $\Delta f_{1,2}$ and $j_{\|}$ must be temporally uncorrelated. To substantiate this, we first plot the ensemble average and standard deviation of $\Delta f_{1,2}(t)$ and $\nabla j_{\|}(t)$ time traces in figures 9(a) and (b) separately in the stable and in the unstable discharges. In the unstable plasmas, we use the last 600 ms data before the 2,1 mode begins to grow. For comparison, we use the last 600 ms before $t = 2000$ ms in the stable shots (measured after the β_N flattop start), which is the average survival time of unstable shots (i.e. the τ parameter of the onset time distribution in figure 3(a)). In accord with analyses of the

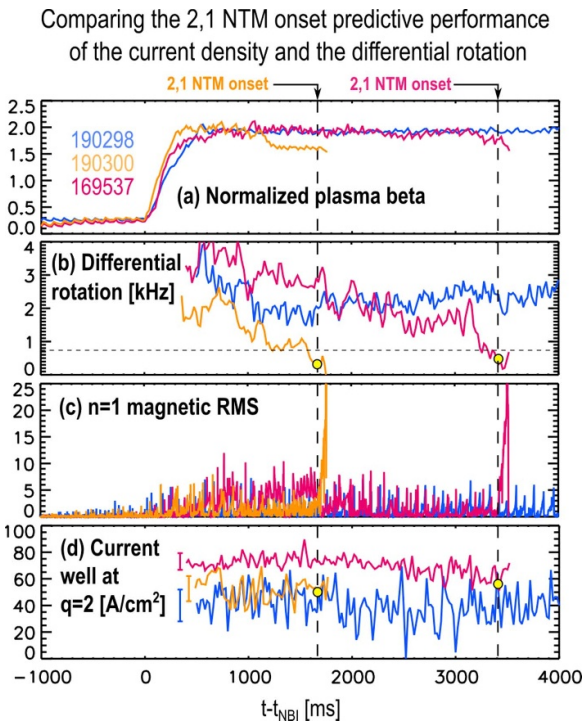

figure 8. Time traces of (*a*) normalized plasma beta, (*b*) differential rotation, (*c*) $n = 1$ magnetic RMS amplitude and (*d*) current well at $q = 2$ in stable and unstable IBS plasmas. Note that these examples are consistent with analyses of the full database shown in figures 5, 6, and 7.

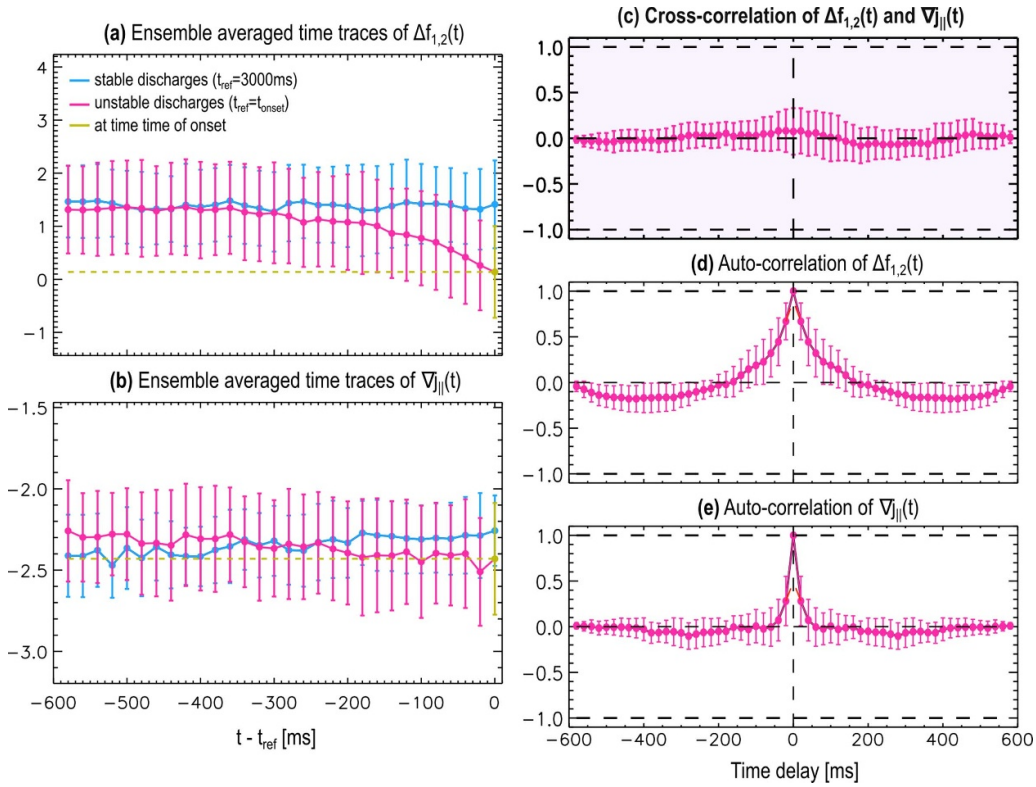

Figure 9. Time traces of (*a*) $\Delta f_{1,2}$ and (*b*) $\nabla j_{\parallel}$ in stable and unstable low-torque IBS plasmas approaching the instability onset. (*c*) Cross-correlation of $\Delta f_{1,2}(t)$ and $\nabla j_{\parallel}(t)$. Auto-correlation functions of (*d*) $\Delta f_{1,2}(t)$ and (*e*) $\nabla j_{\parallel}(t)$.

previous sections, $\Delta f_{1,2}(t)$ drops before the 2,1 island onset, while it is steady in the stable plasmas. While statistical variations between the discharges are relatively large, the trends are clear. $\nabla j_{\parallel}(t)$ does not show systematic changes preceding the island onset in figure 9(*b*).

Next, we calculate the cross-correlation function (CCF(τ)) of $\Delta f_{1,2}(t)$ and $\nabla j_{\parallel}(t)$ of each unstable plasma in the database:

$$\mathrm{CCF}(\tau) = \frac{\int \tilde{\nabla j}_{\parallel}(t+\tau)\,\tilde{\Delta f}_{1,2}(t)\,\mathrm{d}t}{\sqrt{\int \tilde{\nabla j}^2_{\parallel}(t)\,\mathrm{d}t \int \tilde{\Delta f}^2_{1,2}(t)\,\mathrm{d}t}}. \tag{4}$$

Here the time average of each differential rotation and current gradient signal has been subtracted (hence the $\sim$ symbol). The ensemble average (<CCF>) and the standard deviation (σ_{CCF}) of the CCF are calculated as:

$$\begin{aligned} \langle \mathrm{CCF}(\tau)\rangle_s &= \tfrac{1}{N_u}\sum_{k=0}^{N_u} \mathrm{CCF}_k(\tau) \text{ and} \\ \sigma_{\mathrm{CCF}}(r) &= \sqrt{\frac{\sum_{k=0}^{N_u}(\langle \mathrm{CCF}(\tau)\rangle - \mathrm{CCF}_k(\tau))^2}{N_u}}, \end{aligned} \tag{5}$$

where N_u is the number of unstable shots. The same definitions are used to calculate the auto-correlation functions (ACF) of the differential rotation and the current gradient separately. The width of the ensemble averaged ACF of $\Delta f_{1,2}(t)$ in figure 9(*d*) is about 100 ms, confirming that the observed drop before the 2,1 island is statistically significant feature and occurs on roughly the same time-scale in these discharges. In contrast, no statistically significant trend is observed in the evolution of $\nabla j_{\parallel}$. In accord, the ACF of $\nabla j_{\parallel}(t)$ in figure 9(*e*) is close to the ACF of a noise dominated signal, i.e. ACF(0) = 1 but nearly 0 otherwise. Finally, as expected, $\Delta f_{1,2}(t)$ and $\nabla j_{\parallel}(t)$ decouple which is seen from the fact that there is no significant correlation between them as shown by the CCF in figure 9 (*c*).

8. Summary

We presented statistical analyses investigating possible physical mechanisms of disruptive *m,n* = 2,1 tearing mode onsets focusing on the impacts of the rotation and current profiles. In the analysed database of DIII-D ITER baseline scenario discharges, the 2,1 tearing modes most commonly destabilize at the time and frequency of a sawtooth precursor, which is known to exhibit a 2,1 component due to coupling to a 3,2 island or to the Shafranov-shift [13]. The seeding sawtooth is selected by near zero differential rotation. The onset time distribution of these 2,1 tearing modes is nearly exponential and the onset rate is constant in time. The onset empirical probability rapidly increases with the normalized plasma beta and peaks at zero differential rotation, while it appears to only weakly depend on the current gradient at the mode rational surface. There are no statistically significant changes in the magnetic pitch angle and current data between the stable and unstable time-windows. The cross-correlation between the differential rotation and the current gradient is statistically insignificant.

In line with NTM theory, these observations strongly support that most of the 2,1 tearing modes exhibit a finite threshold, are triggered by the sawtooth precursor when the rotation profile flattens, have a near uniform onset rate in time, and are driven by the pressure gradient. On the other hand, lack of statistically significant differences between the current profile of stable and unstable states, as well as lack of correlation between the tearing mode onset rate and the current profile relaxation both reject causality between the current profile evolution and the onset of these disruptive instabilities. These support that preserving the differential rotation between the $q = 1$ and $q = 2$ rational surfaces is key to long pulse stable operation in the plasma scenario planned for ITER, while optimization of the current profile within the explored parameter space may lead to much weaker improvements than sustaining the differential rotation.

Thus, quantitative tearing stability predictions of ITER plasmas calls for modelling the MHD seeding, rotation and polarization current physics.

Acknowledgments

This material is based upon work supported by the U.S. Department of Energy, Office of Science, Office of Fusion Energy Sciences, using the DIII-D National Fusion Facility, a DOE Office of Science user facility, under Awards DE-FC02-04ER54698, DE-AC52-07NA27344, DE-SC0022270 and DE-SC0014264. The data that support the findings of this study are available from the corresponding author upon reasonable request.

Disclaimer

ORCID iDs

L. Bardoczi https://orcid.org/0000-0002-8280-2423
N.J. Richner https://orcid.org/0000-0001-5544-3915
N.C. Logan https://orcid.org/0000-0002-3268-7359
E.J. Strait https://orcid.org/0000-0001-9215-3757
C. Rea https://orcid.org/0000-0002-9948-2649

References

[1] Luce T.C. *et al* 2014 *Expanding the Physics Basis of the Baseline Q = 10 Scenario Toward ITER Conditions* (Bulletin of the International Atomic Energy Agency) PPC/P2- 23
[2] Bardoczi L., La Haye R.J., Strait E.J., Logan N.C., Smith S.P., Richner N.J. and Callen J.D. 2023 *Nucl. Fusion* **63** 096021
[3] Carrera R., Hazeltine R.D. and Kotschenreuther M. 1986 *Phys. Fluids* **29** 899–902
[4] Fietz S., Maraschek M., Zohm H., Reich M., Barrera L. and McDermott R.M. (Mcdermott and the ASDEX Team) 2013 *Plasma Phys. Control. Fusion* **55** 085010
[5] Lazarro E. *et al* 2012 Triggerless onset and effect of 'natural' rotation on neoclassical tearing modes in the TCV Tokamak *Proc. 24th Int. Conf. on Fusion Energy* (*San Diego*, *2012*) p EX/P4-32 (available at: http://www-naweb.iaea.org/napc/physics/FEC/FEC2012/index.htm)
[6] Gerhardt S.P. *et al* 2009 *Nucl. Fusion* **49** 032003
[7] Bardoczi L., Logan N. and Strait E. 2021 *Phys. Rev. Lett.* **127** 055002
[8] Bardoczi L. 2021 *Neoclassical Tearing Mode Seeding by Nonlinear Three-Wave Interactions in Tokamaks* (Bulletin of the American Physical Society, Department of Plasma Physics) GO08.00006
[9] Canal G.P., Duval B.P., Felici F., Goodman T.P., Graves J.P., Pochelon A., Reimerdes H., Sauter O. and Testa D. 2013 *Nucl. Fusion* **53** 113026
[10] La Haye R.J., Chrystal C.C., Strait E.J., Callen J.D., Hegna C.C., Howell E.C., Okabayashi M. and Wilcox R.S. 2022 *Nucl. Fusion* **62** 056017
[11] Strait E.J. 2006 *Rev. Sci. Instrum.* **77** 023502
[12] Urso L., Maraschek M. and Zohm H. the ASDEX Upgrade Team 2005 *J. Phys.: Conf. Ser.* **25** 266
[13] Fitzpatrick R. 2015 *Phys. Plasmas* **22** 042514
[14] Bardoczi L., Podesta M., Heidbrink W.W. and Van Zeeland M.A. 2019 *Plasma Phys. Control. Fusion* **61** 055012
[15] Bardoczi L., Richner N.J. and Logan N.C. 2023 *Nucl. Fusion* **63** 126052
[16] Bardoczi L., Richner N.J., Zhu J., Rea C. and Logan N.C. 2023 *Phys. Plasmas* **30** 092505
[17] Olofsson K.E., Humphreys D.A. and La Haye R.J. 2018 *Plasma Phys. Control. Fusion* **60** 084002
[18] Burrell K.H., Gohil P., Groebner R.J., Kaplan D.H., Robinson J.I. and Solomon W.M. 2004 *Rec. Sci. Instrum.* **75** 3455
[19] Wroblewski D. and Lao L.L. 1992 *Rev. Sci. Instrum.* **63** 5140
[20] Petty C.C., Austin M.E., Holcomb C.T., Jayakumar R.J., La Haye R.J., Luce T.C., Makowski M.A., Politzer P.A. and Wade M.R. 2009 *Phys. Rev. Lett.* **102** 045005
[21] Turco F., Luce T.C., Solomon W., Jackson G., Navratil G.A. and Hanson J.M. 2018 *Nucl. Fusion* **58** 106043
[22] Turco F., Luce T.C., Boyes W., Hanson J. and Hyatt A. 2024 *Nucl. Fusion* **64** 076048
[23] Callen J.D., La Haye R.J. and Strait E.J. 2021 *Tearing Modes in IBS Discharges, CTMs or NTMs?* (Bulletin of the American Physical Society, Department of Plasma Physics) GP11.00033